Article

Journal of
Nanoscience and Nanotechnology
Vol. 19, 1425–1431, 2019
www.aspbs.com/jnn

Improved pH Sensitivity and Reliability for Extended Gate Field-Effect Transistor Sensors Using High-*k* Sensing Membranes

Joo-Won Kang and Won-Ju Cho*

Department of Electronic Materials Engineering, Kwangwoon University, 20 Kwangwoon-ro, Nowon-Gu, Seoul 01897, Republic of Korea

In this study, we fabricated extended-gate (EG) field-effect transistor (FET) pH sensors with dual-gate (DG) structures, using a range of dielectric sensing membranes (SiO_2, Si_3N_4, HfO_2 and Ta_2O_5) to vary their sensitivity. The fabricated EGFETs consisted of a silicon-on-insulator (SOI)-based metal-oxide semiconductor field-effect transistor (MOSFET) transducer and an EG sensor. We amplified the sensitivity of the device far beyond the Nernst limit (59 mV/pH), which is the theoretical maximum of conventional ion-selective FET (ISFET) sensing, by applying capacitive coupling. Among the evaluated dielectric sensing membranes, we obtained the highest sensitivity (478 mV/pH), low hysteresis (100.2 mV) and drift rate (24.6 mV/h) from the pH sensor with a Ta_2O_5 membrane. Hence, we expect DG FET configurations using Ta_2O_5 films as EG sensing membranes to be useful for high performance biosensor applications, as they satisfy the requirements for sensitivity, stability and reliability.

Keywords: Dual-Gate Field-Effect Transistor, Ion-Sensitive Field-Effect Transistor, pH Sensor, Capacitive Coupling, High-*k* Sensing Membrane, Sensitivity.

1. INTRODUCTION

Research in the field of biosensors has increased enormously, as the quality of life of the general public, and the interest in improving public health, has increased. Recent advances in biosensor technologies have the potential to deliver point-of-care diagnostics that match or surpass conventional standards, with respect to time, accuracy, and cost. Modern biosensors are broadly classified as label or label-free sensing devices, and are manufactured using microfabrication and nanofabrication methods. In general, biosensors consist of sensing and transducing components. The sensing part of these devices detects biochemical elements such as tissue, microorganisms, DNA, enzymes, antibodies, and pH, while the transducing part converts the signal resulting from the interaction of the analyte with the sensing components into a different signal that can be more easily measured and quantified. Typical transducers for biological events include surface plasmon resonance, electrochemical and optical responses, and potentiometric responses based on field-effect transistors (FETs).[1, 2]

Of the possible transducing technologies, low-cost ion-sensitive FETs (ISFETs), which can easily be integrated with CMOS devices because of their comparable fabrication processes, are widely-used as a representative biosensor, due to their real-time label-free selective detection of biological analytes in a solution.[1] Conceptually, the ISFET is a metal-oxide semiconductor field-effect transistor (MOSFET), in which the metal gate electrode has been removed, such that the oxide layer is directly exposed to the electrolyte for which the specific ion concentration is to be measured. Instead of a fixed metal gate, a reference potential is applied to the electrolyte-oxide-semiconductor system through a reference electrode.[1] The concentration of H^+ ions in the electrolyte directly affects the surface potential of the oxide film, which changes the threshold voltage of the ISFET, causing the ion sensitivity of the drain current.[2] Using these mechanisms, ISFET-based biosensors that react to specific antibodies, urea, and glucose have been studied.[3–6]

Since the electrical potential generated by actual biological events is very low, a biosensor with a sensitivity higher than the Nernst limit for conventional ISFETs (59 mV/pH) is essential, for the creation of commercially

*Author to whom correspondence should be addressed.

viable devices.[7] To this end, an atypical ISFET, with a dual-gate (DG) structure, has been proposed. With DG ISFET sensors, the Nernst limit can easily be overcome without additional circuitry or components,[8–12] as the sensitivity of these devices is amplified by the capacitive coupling effect, a phenomenon that occurs between the upper and lower insulating films of a channel, and was first quantitatively analyzed in silicon-on-insulator (SOI) transistors by the Fossum group in 1983.[13]

A secondary factor that limits the commercialization of ISFET-based sensors is reliability, as devices in which the detector and transducer elements are combined can no longer be used if the sensing membrane is damaged in solution. Extended-gate (EG) FETs with separate detectors and transducers have thus been proposed as more economical sensing options.[14–20] With this kind of device, damaged sensing membranes (EGs) can be replaced, enabling the creation of cost-effective disposable sensors.

In this study, to develop a pH sensor with a high sensitivity, we investigated suitable sensing membranes, including materials with large electrical permittivity (high-*k*), for EGFETs with DG structures, by employing SiO_2, Si_3N_4, HfO_2, and Ta_2O_5 as dielectric layers. We fabricated these pH sensors by connecting the EG, with the sensing membrane deposited on an ITO-coated glass substrate, to an SOI MOSFET. The dielectric constants of the sensing membranes were measured in a metal-insulator-metal (MIM) capacitor configuration. The capacitive coupling

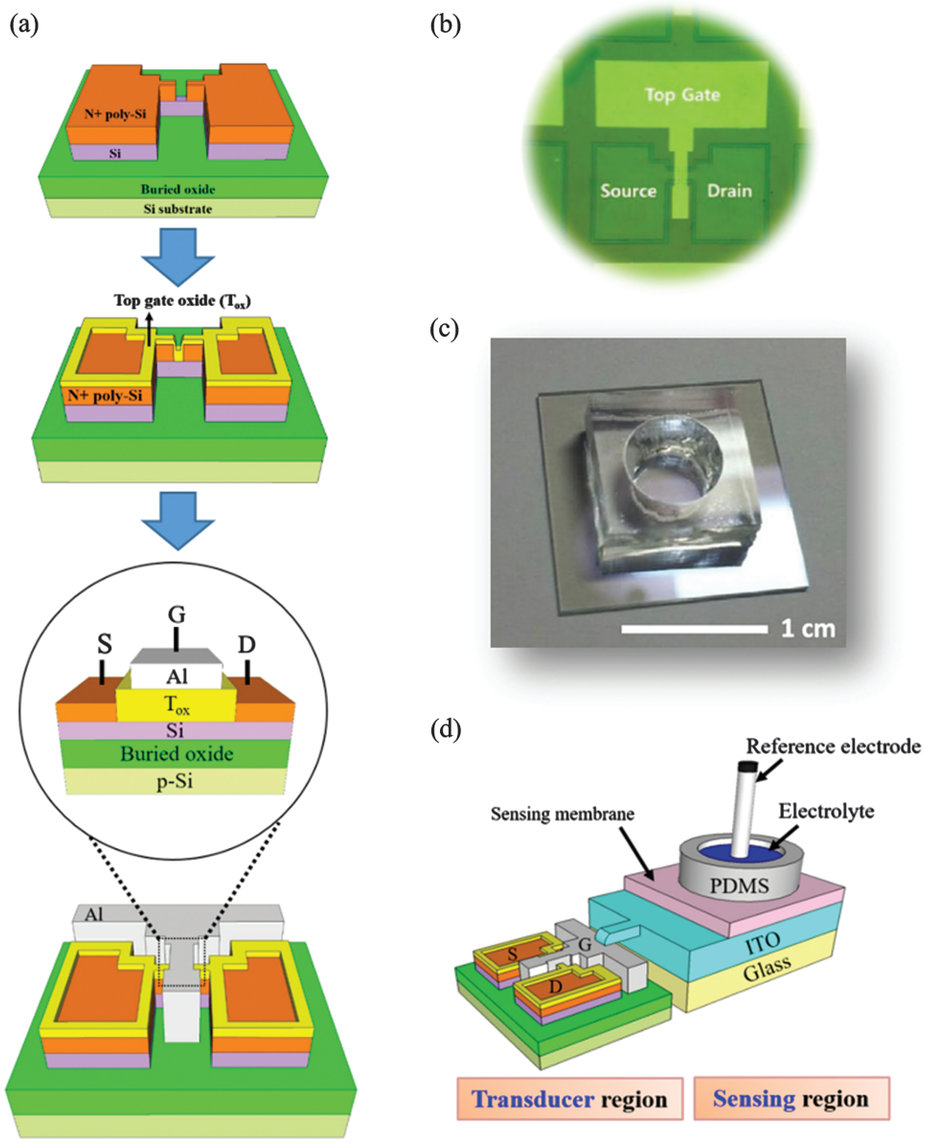

Figure 1. (a) Schematic depicting the fabrication flow and structure of the DG FETs. (b) Optical micrograph of the top view of the fabricated DG FETs. (c) Photograph of the fabricated EG. (d) Schematic diagram of a fabricated sensor, illustrating the connection of the DG FET to the EG.

effect of the DG EGFET was quantified for each sensing membrane, and the sensitivity of the device in SG-mode and DG-mode was evaluated. In addition, we measured the hysteresis and the drift characteristics of each device, to evaluate the reliability and stability of the sensing membranes.

2. EXPERIMENTAL DETAILS

2.1. Transducer Fabrication

The fabrication process for the DG-type FET transducers, and the schematic structure of the devices, is illustrated in Figure 1(a). The transducers were fabricated on a fully depleted *p*-type (100) SOI wafer with a doping concentration of 1×10^{15} cm^3, a 200-nm-thick buried oxide (BOX) layer, and a 100-nm-thick top silicon layer. Following a standard RCA cleaning process, the active regions of the SOI MOSFETs were patterned using photolithography and reactive ion etching (RIE). A 100-nm-thick phosphorus-doped n^+ poly-Si layer was subsequently deposited at the source/drain (S/D) region, using low-pressure chemical vapor deposition (LPCVD). The lengths and widths of the active channels of the DG FETs were designed to be 20 μm and 10 μm, respectively. A 20-nm-thick SiO_2 layer was deposited using radio-frequency (RF) magnetron sputtering, for the top gate oxide layer of the DG FETs. Then, a rapid thermal annealing (RTA) treatment was performed at 950 °C for 30 s in N_2 ambient, for activation of the dopant in the S/D region. Following deposition of a 150-nm-thick aluminum layer, using an e-beam evaporator system, for the gate electrode and S/D contacts, we conducted a forming gas annealing treatment at 450 °C for 30 min in a 2% H_2/N_2 ambient, to improve the electrical properties of the DG FETs. Figure 1(b) depicts an optical micrograph of the top view of the fabricated DG FETs.

2.2. Detector Fabrication

To transmit the change in the surface potential of the sensing membrane to the metal gate electrode on the transducer, a 100-nm-thick indium-tin oxide (ITO) film was deposited on a clean glass substrate using RF magnetron sputtering, at room temperature. Subsequently, 50-nm-thick SiO_2, Si_3N_4, HfO_2, and Ta_2O_5 films were deposited on the ITO layer, as sensing membranes. We sputtered these films at an RF power of 50 W, with an Ar flow rate of 20 sccm in a chamber pressurized to 3 mTorr. The dielectric constants of the sensing membranes, measured in the metal-insulator-metal (MIM) capacitor configuration, were 3.7, 7.6, 17.8, and 26.9 for SiO_2, Si_3N_4, HfO_2, and Ta_2O_5, respectively. The ITO electrode in the sensing area was connected directly to the aluminum top gate electrode in the transducer using a cable wire. Finally, a polydimethylsiloxane (PDMS) chamber with an internal diameter of 0.6 cm, where the pH solution was injected, was attached to the sensing membrane using silicone glue. A photograph of the fabricated EG is shown in Figure 1(c). Figure 1(d) shows a schematic illustration of the complete sensor, including the connection of the DG FET to the EG.

2.3. Device Characterization

The current–voltage (I–V) and capacitance–voltage (C–V) characteristics of the fabricated devices were measured using an Agilent 4156B semiconductor parameter analyzer, and an Agilent 4284A LCR meter, respectively. We used a commercial Ag/AgCl reference electrode (Horiba 2080A-06T), with a ceramic-plug junction and an internal solution saturated with KCl and AgCl, for pH sensing. We characterized the fabricated DG EGFET pH sensor in two modes of operation: SG-mode and DG-mode. As shown in Figure 2(a), SG-mode sensing was performed by applying a voltage to the top reference electrode, with the bottom gate grounded. In contrast,

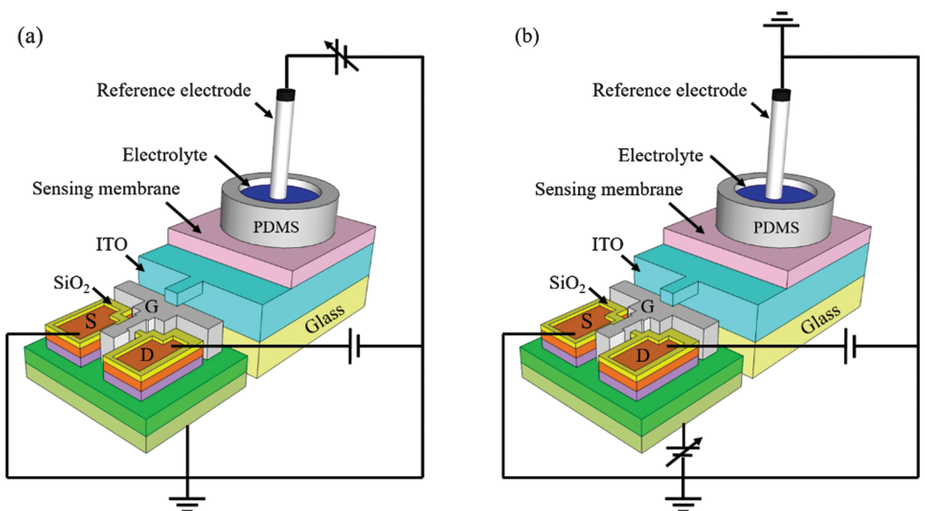

Figure 2. Schematic diagrams illustrating electrical connections for (a) SG-mode sensing, and (b) DG-mode sensing.

DG-mode sensing was performed by applying a voltage to the bottom gate with the top reference electrode grounded, as shown in Figure 2(b).

The sensitivity of each mode was extracted by observing the shift in reference voltage (V_R) at a drain current of 1 nA, with respect to the strength of the pH buffer. We also measured hysteresis and drift characteristics, to evaluate the stability and reliability of the device. We defined the hysteresis voltage (V_H) as the difference between the values of V_R obtained at the first and last pH 7 states a of a 7–10–7–4–7 pH loop. We measured V_R five times per pH, at 2 min intervals, to monitor possible changes in sensor output. To measure the drift characteristics of the device, we observed the variation of V_R during a 10 h measurement of a pH 7 buffer.

3. RESULTS AND DISCUSSION

Figure 3 shows the transfer characteristics of the SOI-based DG FETs with a voltage swept across the top-gate (Fig. 3(a)), and the bottom-gate (Fig. 3(b)). The electrical parameters of these devices are summarized in Table I. For top-gate biasing, we observed a threshold voltage (V_T) of −0.04 V, a subthreshold swing (SS) of 75.20 mV/dec, and an on-off current ratio (I_{on}/I_{off}) of 4.78×10^7. With bottom-gate biasing we observed a V_T of −0.8 V, an SS of 721.5 mV/dec, and an I_{on}/I_{off} of 3.39×10^7. The field-effect mobility of charge carriers can be calculated from the transfer curves, using the following equations:

$$\mu_{FE} = \frac{Lg_m}{WC_{ox}V_D}, \quad g_m = \left.\frac{\partial I_D}{\partial V_G}\right|_{V_D=\text{const}} \tag{1}$$

where W, L, C_{OX}, and g_m are the channel width, length, gate oxide capacitance, and the mutual conductance, respectively. I_D is the drain current and V_G is the gate voltage. The extracted field-effect mobilities were 483.8 and 610.1 $cm^2/V \cdot s$ for top-gate and bottom-gate operation, respectively, with a drain voltage (V_D) of 50 mV. We found that the fully depleted SOI MOSFETs had excellent characteristics in both modes of operation, providing transducer performance suitable for stable DG-mode sensing.

Table I. Electrical parameters of the fabricated SOI MOSFET devices.

Operation mode	Threshold voltage (V)	Field-effect mobility ($cm^2/V \cdot s$)	Subthreshold swing (mV/dec)	On–off current ratio
Top-gate	−0.04	483.8	75.2	4.8×10^7
Bottom-gate	−0.8	610.1	721.5	8.1×10^7

We performed further experiments to evaluate the performance of the EGs as sensors. Table II summarizes the characteristics of the different sensing membranes, operating in SG-mode and DG-mode. Figure 4 shows the transfer characteristics of devices with different sensing membranes operating in SG-mode, in a range of pH buffers. The sensitivity of the devices was calculated from the transfer curve measured at $V_D = 0.5$ V, using the shift in V_R observed at a drain current (I_D) of 1 nA. The insets in this figure show the $\Delta V_R/\Delta pH$ characteristics from which the pH sensitivities of the different membranes were extracted. In SG-mode, the sensitivities of the SiO_2, Si_3N_4, HfO_2, and Ta_2O_5 membranes were 36, 52.8, 54.6, and 56 mV/pH, respectively, which do not exceed the Nernst limit (∼59 mV/pH). We observed a tendency for the pH sensitivity to increase with dielectric constant.

To overcome the Nernst limit, which is a requirement for practical biosensor application,[7] we made use of the amplification caused by the capacitive coupling effect generated in DG-structure FETs, by changing the mode of operation. Figure 5 shows the transfer characteristics of devices with different sensing membranes operating in DG-mode, in a range of pH buffers. We observed a greater shift in transfer curves with respect to the strength of the pH buffer, in contrast to SG-mode, due to the capacitive coupling phenomenon. This is because the sensitivity of the device in SG-mode depends only on the change in the surface potential of the sensing membrane, whereas the sensitivity in DG-mode is dependent on both the surface potential of the sensing membrane and the bias of the bottom gate. The relationship between sensitivity and

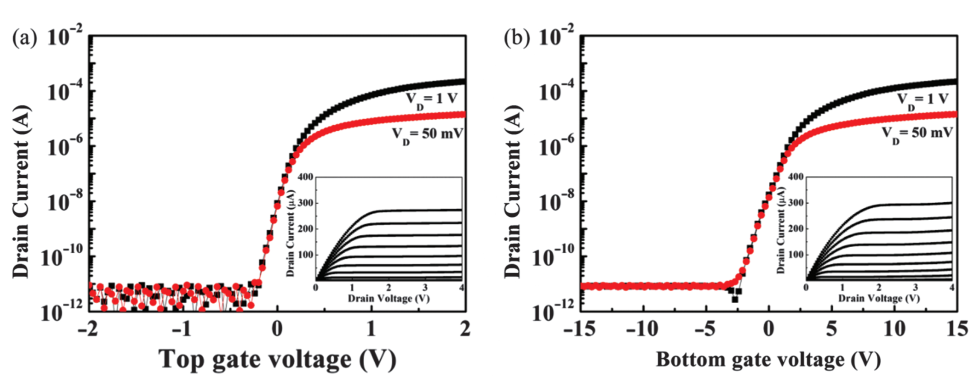

Figure 3. Transfer characteristics of SOI-based DG FETs in (a) top-gate and (b) bottom-gate operation. Insets show output characteristic curves. V_G–V_T = 0–2 V for top gate operation, and 0–15 V for bottom gate operation.

Table II. Sensing performance characteristics of different membranes operating in SG-mode and DG-mode.

Sensing membrane	SG-mode sensitivity (mV/pH)	SG-mode linearity (%)	DG-mode sensitivity (mV/pH)	DG-mode linearity (%)	DG/SG sensitivity
SiO_2	36.0	99.55	356.1	98.93	9.9
Si_3N_4	52.8	99.85	398.3	98.23	7.5
HfO_2	54.6	99.69	438.8	99.46	8
Ta_2O_5	56.0	99.88	478	99.57	8.5

capacitive coupling can be explained by the following equation:[9]

$$\Delta V_{th}^{B} = \frac{C_{top}}{C_{bottom}} \Delta V_{th}^{T} \tag{2}$$

where C_{top} and C_{bottom} are the capacitances of the top-gate and bottom-gate, respectively, per unit area, and ΔV_{th}^{B} and ΔV_{th}^{T} are the respective shifts in the threshold voltage at the top-gate and bottom-gate. Hence, C_{top}/C_{bottom} is the amplification factor for sensitivity in DG-mode. The sensitivities of the SiO_2, Si_3N_4, HfO_2, and Ta_2O_5 membranes in DG-mode were 359.5, 398.3, 438.8, and 478 mV/pH, respectively, which exceed the Nernst limit. In addition, membrane sensitivity increased with increasing dielectric constant, with Ta_2O_5 exhibiting higher sensitivity than other dielectric layers.

To verify the capacitance coupling effect, we compared the experimental and theoretical values of the amplification factor. In the SOI-based DG FETs used as transducers in this experiment, the ratio of top-gate to bottom-gate capacitance is 10, which is the theoretical sensitivity amplification factor. The ratio of DG sensitivity to SG sensitivity (DG/SG) obtained from the experiment varied between 7.8∼9.9, a range of values which is similar to the theoretical amplification factor, indicating that capacitance coupling is responsible for the improved sensitivity. Hence, as the Ta_2O_5 sensing membrane, with a high dielectric constant, exhibited a sensitivity close to the Nernst limit in SG-mode, this membrane also had the highest sensitivity in DG-mode, due to the capacitive coupling effect.

Finally, we investigated the performance of the sensors with respect to reliability and stability. As previously stated, we defined V_H as the difference between the values of V_R obtained at the first and last pH 7 states of a 7–10–7–4–7 pH loop. This hysteresis effect is caused by the presence of interior sites in the sensing membrane, which are able to react with ions in the pH solution.[21,22] In addition, a relatively slow chemical reaction occurs at the interface of the electrolyte and the surface of the sensing membrane. This chemical reaction changes the capacitance of the insulator surface, and the total insulation capacitance, due to the combination of the equivalent capacitance of the surface layer with the capacitance of the insulator.[23] As a result, the I_D and V_R of the FET transducer vary during prolonged operation. This phenomenon is termed the drift effect, and affects the

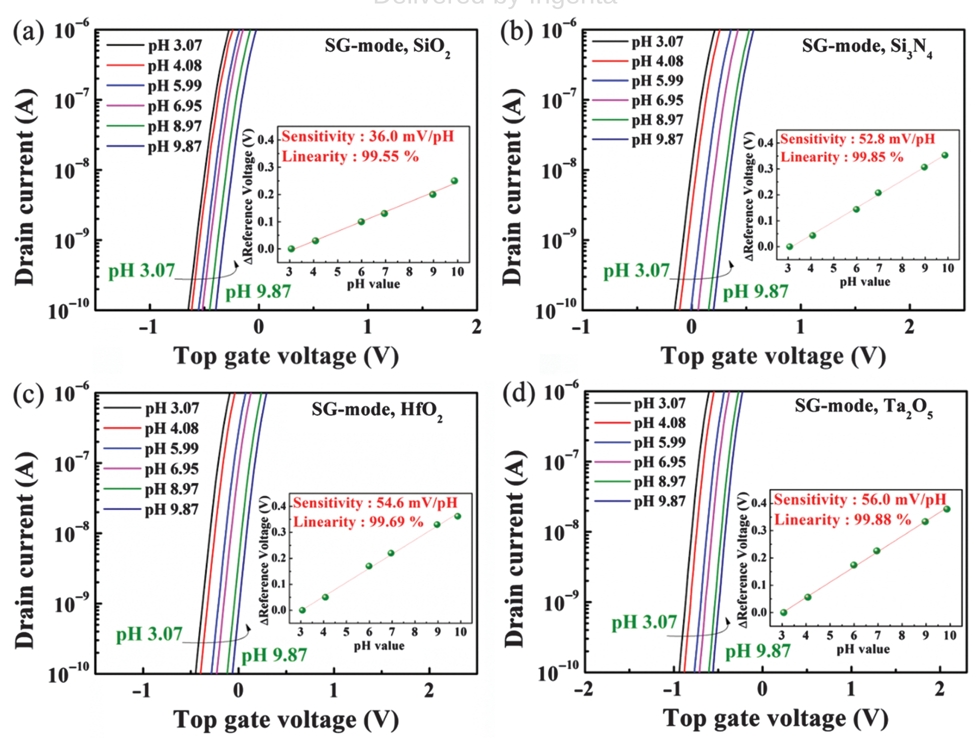

Figure 4. Transfer characteristics of the sensor operating in SG-mode in a range of pH buffers with: (a) SiO_2, (b) Si_3N_4, (c) HfO_2, and (d) Ta_2O_5 sensing membranes. The reference voltage (V_R) of the sensor in each pH buffer, shown in the inset, is defined as the gate voltage corresponding to a drain current (reference current) of 1 nA.

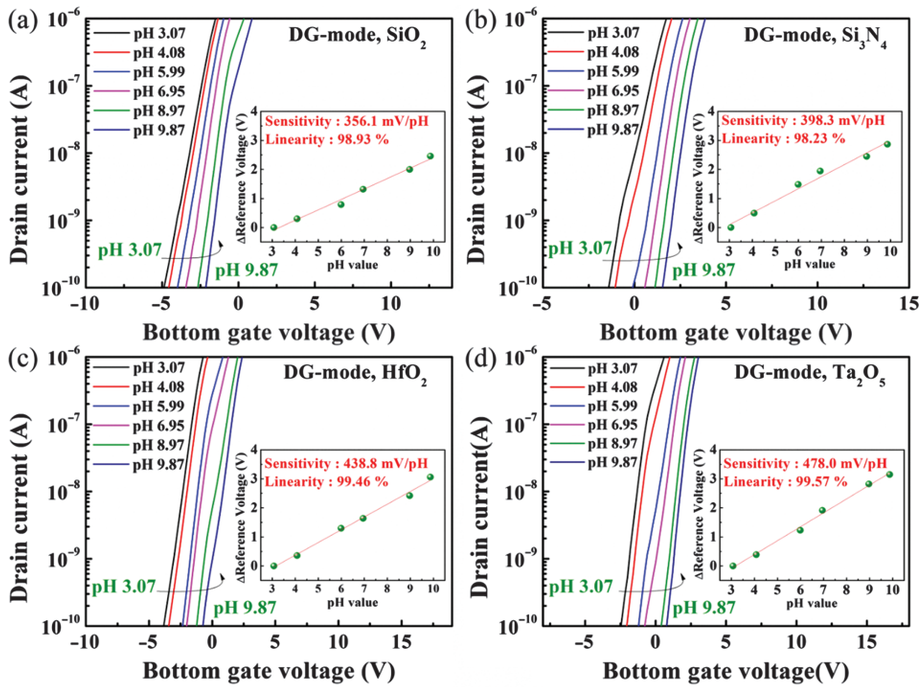

Figure 5. Transfer characteristics of the sensor operating in DG-mode in a range of pH buffers with: (a) SiO_2, (b) Si_3N_4, (c) HfO_2, and (d) Ta_2O_5 sensing membranes. The V_R of the sensor in each pH buffer, shown in the inset, is defined as the gate voltage corresponding to a drain current (reference current) of 1 nA.

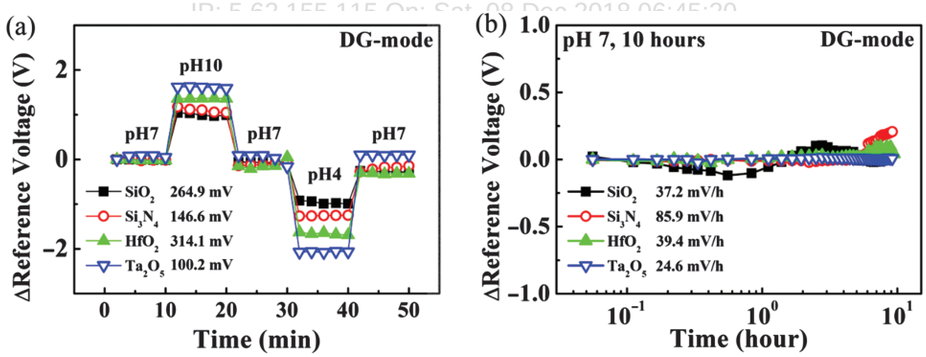

Figure 6. (a) Hysteresis and (b) drift effects for different sensing membranes, with the device operating in DG-mode. V_R is defined as the gate voltage corresponding to a drain current (reference current) of 1 nA.

long-term reliability of the sensor. Figure 6 illustrates the non-ideal effects observed with the different sensing membranes operating in DG-mode. Hysteresis and drift effects are shown in Figures 6(a) and (b), respectively. The measurement shows that the Ta_2O_5 sensing membrane has a V_H of 100.21 mV, and a drift rate of 24.65 mV/h, which is superior to the other sensing membranes investigated.

4. CONCLUSION

In this study, we fabricated a DG SOI EGFET pH sensor, using a range of dielectric films (SiO_2, Si_3N_4, HfO_2, and Ta_2O_5) as sensing membranes. We amplified the sensitivity of these devices using the capacitive coupling effect that occurs between the upper and lower insulating films of the channel, and evaluated the characteristics of the different sensing membranes. Our experiments showed that in SG-mode, the sensitivity the devices approached the Nernst limit as the dielectric constant of the sensing film increased. In DG-mode, we obtained a sensitivity of 478 mV/pH with the Ta_2O_5 sensing film, due to the capacitive coupling effect. In addition, we evaluated the reliability and stability of the fabricated devices in DG-mode, by measuring the hysteresis and drift effects. From these experiments, we observed that the Ta_2O_5 layer, with the largest dielectric constant, showed the highest sensitivity, and lowest hysteresis and drift rate.

Hence, because of the stability and reliability exhibited, we expect DG FET sensor configurations using Ta_2O_5 sensing membranes for the EG to be useful for high performance biosensor applications.

Acknowledgments: This study was supported by the Basic Science Research Program through the National Research Foundation of Korea (NRF) funded by the Ministry of Education, Science, and Technology (No. 2016R1A2B4008754) and conducted with the support of the business Start-up Technology Development Project funded by the Small and Medium Business Administration (SMBA, Korea) in 2016 (Grant No. S2409184).

References and Notes

1. P. Bergveld, *IEEE Trans. Biomed. Eng.* 5, 342 (**1972**).
2. P. Bergveld, *Sensors and Actuators B Chem.* 88, 1 (**2003**).
3. H. I. Seo, C. S. Kim, B. K. Sohn, T. Yeow, M. T. Son, and M. Haskard, *Sens. Actuators B Chem.* 40, 1 (**1997**).
4. C. Puig-Lleixà, C. Jiménez, J. Alonso, and J. Bartrolı, *Anal. Chim. Acta* 389, 179 (**1999**).
5. B. K. Sohn, B. W. Cho, C. S. Kim, and D. H. Kwon, *Sens. Actuators B Chem.* 41, 7 (**1997**).
6. T. Kullick, M. Beyer, J. Henning, T. Lerch, R. Quack, A. Zeitz, B. Hitzmann, T. Scheper, and K. Schürgerl, *Anal. Chim. Acta* 296, 263 (**1994**).
7. O. Knopfmacher, A. Tarasov, W. Fu, M. Wipf, B. Niesen, M. Calame, and C. Schonenberger, *Nano Lett.* 10, 2268 (**2010**).
8. J. K. Park, H. J. Jang, J. T. Park, and W. J. Cho, *Solid-State Electron.* 97, 2 (**2014**).
9. H. J. Jang and W. J. Cho, *Sci. Rep.* 4, 5284 (**2014**).
10. H. J. Jang, J. G. Gu, and W. J. Cho, *Sensors and Actuators B Chem.* 181, 880 (**2013**).
11. I. K. Lee, K. H. Lee, S. Lee, and W. J. Cho, *ACS Appl. Mater. Interfaces* 6, 22680 (**2014**).
12. M. Spijkman, E. C. P. Smits, J. F. M. Cillessen, F. Biscarini, P. W. M. Blom, and D. M. de Leeuw, *Appl. Phys. Lett.* 98, 043502 (**2011**).
13. H. K. Lim and J. G. Fossum, *IEEE Trans. Electron Devices* 30, 1244 (**1983**).
14. L. L. Chi, J. C. Chou, W. Y. Chung, T. P. Sun, and S. K. Hsiung, *Mater. Chem. Phys.* 63, 19 (**2000**).
15. J. C. Chen, J. C. Chou, T. P. Sun, and S. K. Hsiung, *Sens. Actuators B Chem.* 91, 180 (**2003**).
16. T. Sakata, S. Matsumoto, Y. Nakajima, and Y. Miyahara, *Jpn. J. Appl. Phys.* 44, 2860 (**2005**).
17. P. D. Batista and M. Mulato, *Appl. Phys. Lett.* 87, 143508 (**2005**).
18. L. T. Yin, J. C. Chou, W. Y. Chung, T. P. Sun, and S. K. Hsiung, *Sens. Actuators B Chem.* 71, 106 (**2000**).
19. Y. L. Chin, J. C. Chou, Z. C. Lei, T. P. Sun, W. Y. Chung, and S. K. Hsiung, *Jpn. J. Appl. Phys.* 40, 6311 (**2001**).
20. H. H. Li, C. E. Yang, C. C. Kei, C. Y. Su, W. S. Dai, J. K. Tseng, P. Y. Yang, J. C. Chou, and H. C. Cheng, *Thin Solid Films* 529, 173 (**2013**).
21. S. P. Chang and T. H. Yang, *Int. J. Electrochem. Sci.* 7, 5020 (**2012**).
22. L. Bousse, S. Mostarshed, B. van der Schoot, and N. F. De Rooij, *Sen. Actuators B Chem.* 17, 157 (**1994**).
23. L. Bousse and P. Bergveld, *Sens. Actuators* 6, 65 (**1984**).

Received: 10 December 2017. Accepted: 19 March 2018.